ARTICLE

Check for updates

Polarisation-dependent single-pulse ultrafast optical switching of an elementary ferromagnet

Hanan Hamamera [1,2✉], Filipe Souza Mendes Guimarães [3], Manuel dos Santos Dias [1] & Samir Lounis [1,4✉]

The ultimate control of magnetic states of matter at femtosecond (or even faster) timescales defines one of the most pursued paradigm shifts for future information technology. In this context, ultrafast laser pulses developed into extremely valuable stimuli for the all-optical magnetization reversal in ferrimagnetic and ferromagnetic alloys and multilayers, while this remains elusive in elementary ferromagnets. Here we demonstrate that a single laser pulse with sub-picosecond duration can lead to the reversal of the magnetization of bulk nickel, in tandem with the expected demagnetization. As revealed by realistic time-dependent electronic structure simulations, the central mechanism involves ultrafast light-induced torques that act on the magnetization. They are only effective if the laser pulse is circularly polarized on a plane that contains the initial orientation of the magnetization. We map the laser pulse parameter space enabling the magnetization switching and unveil rich intra-atomic orbital-dependent magnetization dynamics featuring transient inter-orbital non-collinear states. Our findings open further perspectives for the efficient implementation of optically-based spintronic devices.

[1] Peter Grünberg Institut and Institute for Advanced Simulation, Forschungszentrum Jülich & JARA, 52425 Jülich, Germany. [2] Department of Physics, RWTH Aachen University, 52056 Aachen, Germany. [3] Jülich Supercomputing Centre, Forschungszentrum Jülich & JARA, 52425 Jülich, Germany. [4] Faculty of Physics, University of Duisburg-Essen & CENIDE, 47053 Duisburg, Germany. ✉email: h.hamamera@fz-juelich.de; s.lounis@fz-juelich.de

The manipulation and control of magnetic materials by ultrashort laser pulses have been extensively researched since the discovery of optically driven ultrafast demagnetization in nickel[1]. The technological potential of this discovery was quickly recognized, leading to proof-of-concept experiments in connection with information storage[2–4]. Such laser-driven magnetization dynamics have also been explored in bulk rare-earth ferromagnets[5], in ferrimagnets[2,6–13], and in ferromagnetic thin films[3,14–23]. The underlying physical picture is not yet fully understood, given the diversity of mechanisms that can contribute to or influence the dynamics on distinct or overlapping time scales[24–27].

For applications, the goal is not simply to change or demagnetize the material but to controllably reverse the magnetization direction, which encodes an information bit. This has been successfully achieved in GdFeCo thanks to its ferrimagnetism[2,9]. For this material, the magnetization switching is due to laser-driven heating above the ferrimagnetic compensation point[9], together with the different relaxation time scales of the two rare-earth and transition metal sublattices[6], and only weakly depends on the polarization of the laser[8]. Magnetization switching has also been demonstrated for ferromagnetic Co/Pt multilayers, where the helicity of the laser is an important factor to achieve deterministic switching. While GdFeCo can be switched with a single pulse, for Co/Pt several long pulses[19] or hundreds of short pulses[28] are needed to achieve full switching—which is detrimental for technological applications due to the high-energy consumption and the relative slowness of the whole process. It has been recently reported that only two laser pulses are enough to achieve complete helicity-dependent switching in Co/Pt[20].

In order to make progress and to understand how to achieve full switching in a ferromagnet with a single laser pulse, the appropriate physical mechanism or combination of physical mechanisms have to be identified and simulated. The three-temperature model[1,25,29,30] describes the nonequilibrium thermodynamics of coupled electronic, magnetic and lattice subsystems, and provides a very good semi-phenomenological description of the demagnetization of bulk Ni. It can also be generalized to describe the switching of ferrimagnetic GdFeCo[31]. Demagnetization and switching due to the stochastic magnetization dynamics are driven by laser heating of the material were studied numerically using Landau–Lifshitz–Gilbert and Landau–Lifshitz–Bloch equations[6,9,32,33]. There are also several proposed microscopic pictures for how the electrons react to the laser and lead to ultrafast demagnetization. The inverse Faraday effect (IFE) was proposed as a direct mechanism for laser-induced demagnetization[34], which evolved into a more general picture of light-induced magnetic torques[35–40]. The superdiffusive spin transport model[41] introduces spin-polarized hot electrons that transfer angular momentum from the magnetic atoms to a non-magnetic material. Mechanisms for demagnetization due to the transfer of angular momentum from the spins to the lattice have also been extensively studied[5,42–45]. Simulations considering electron–electron interactions[46] identified a three-step mechanism: the laser pulse creates electron–hole excitations, spin–orbit coupling (SOC) converts the excited spin to orbital angular momentum, and the latter is then quickly quenched by the lattice. Lastly, time-dependent density functional theory (TDFT) simulations of the combined dynamics of the electrons and the magnetic moments that they form have yielded many microscopic insights into the ultrafast demagnetization in the sub-100 fs regime[17,18,44,47–51].

So far all the simulations based on a realistic description of the electronic structure were limited to ultrafast demagnetization processes. Here we address all-optical magnetization reversal and the possibility of inducing it with a single laser pulse in an elementary ferromagnet such as face fcc bulk Ni. We employ a recently developed time-dependent tight-binding framework parameterized from density functional theory (DFT) calculations, with a specific algorithm enabling us to monitor the non-linear magnetization dynamics up to a few picoseconds. We show that a single laser pulse can trigger the magnetization reversal of Ni, for which we identified the pulse parameter space enabling magnetization switching summarized in Fig. 1. We identify ultrafast light-induced torques as the underlying mechanism, which acts on the magnetization if the polarization of the pulse obeys specific conditions. We found strong non-collinear, ferromagnetic and antiferromagnetic intra-atomic transient states that are shaped by the interplay of optical inter-orbital electronic transitions and spin–orbit induced spin–flip processes.

Results

All-optical magnetization reversal. We perform tight-binding simulations parameterized from DFT by propagating the ground state eigenvectors in real-time solving the time-dependent Schrödinger equation up to a few picoseconds. Our Hamiltonian includes the kinetic energy as given by the electronic hopping, the SOC, the electron–electron exchange interactions, and the effect of the laser-induced excitations. The propagated solutions
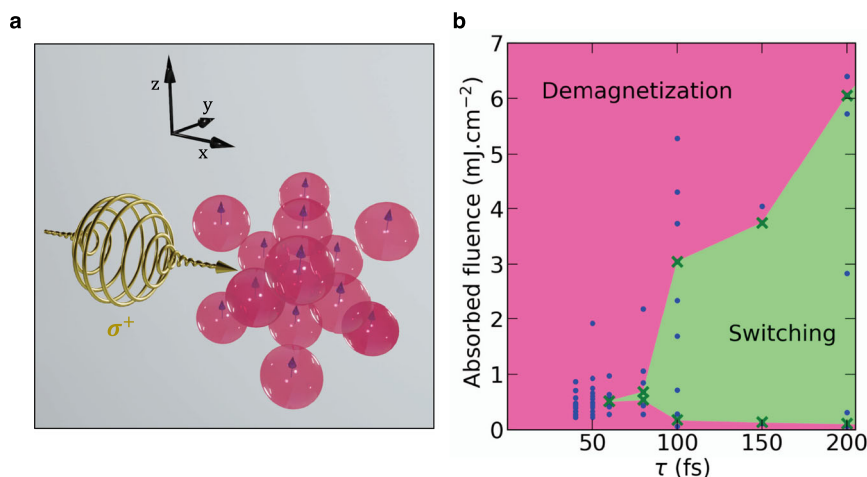

Fig. 1 Parameter space for single-pulse all-optical switching of bulk Ni. a Schematic representation of a circular light pulse interacting with an fcc bulk material with initial magnetization pointing along the +z direction. **b** Laser parameter phase diagram for bulk Ni as a function of the laser pulse width τ and absorbed fluence. The dots indicate all the performed calculations, and the crosses mark the identified boundaries.
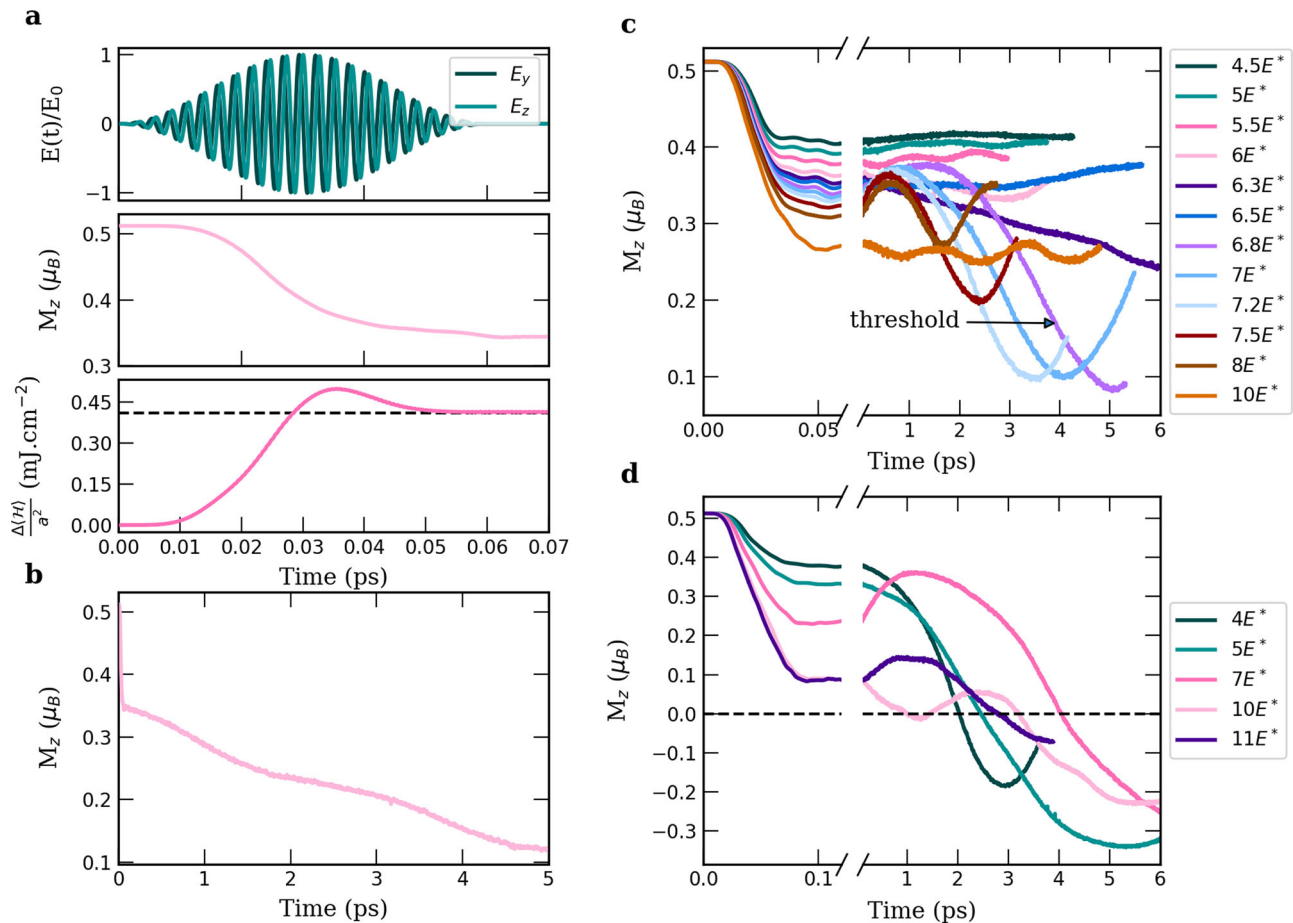
Fig. 2 Diversity of laser-induced magnetization dynamics in bulk Ni. a A 60 fs-wide pulse with the intensity of $E_0 = 6E^*$, the demagnetization (M_z) in Bohr magneton (μ_B) that it induces, and the energy ($\frac{\Delta \mathcal{H}}{a^2}$) absorbed during its application where a is the lattice constant. The x-axis in all sub-figures represents the integration time in picoseconds. **b** Evolution of the M_z component for longer times. **c** Demagnetization curves for a 50 fs-wide pulse with different laser field intensities. **d** Switching is observed for a 100 fs-wide pulse for different laser field intensities. The reference value for the laser field intensity is $E^* = 9.7 \times 10^8$ V m^{-1}.

were then used to calculate the longitudinal and transverse components of the magnetization as well as the absorbed energy together with the redistribution of the electronic population among the different orbitals. Within our method, the time evolution of the wavefunctions is stable up to a few ps, enabling us to use large pulse widths (up to 1 ps) to investigate the effect of both linearly and circularly polarized pulses over a long time scale (see the "Methods" section for more details).

In the ground state of bulk Ni, the spin moment is found to be $0.51\mu_B$ and prefers to point along the cubic axes. Here, we assume it to point along the [001] direction, which we choose to be the z cartesian axis. We then systematically apply single optical pulses while tracking the time-dependent magnetization dynamics of the system. The pulses have a fixed frequency $\omega = 1.55$ eV$\hbar^{-1}$ and varying widths and intensities of the electric field E_0, and we consider both linear and circular polarized light (see schematic Fig. 1a and "Methods" section for more details).

As a first example, Fig. 2a displays the electric field components of a 60 fs laser pulse circularly polarized in the yz-plane (see the "Methods" section for the precise form of the pulse), as well as the time-dependent reduction of the z-component of the Ni spin moment, and the absorbed laser fluence that we approximate by the change in the energy of the material divided by its cross-section. Up to 70 fs, we recover the usual demagnetization pattern characterizing Ni. A reduction of about 30% is found when the

absorbed laser fluence reaches 0.41 mJ cm^{-2} at the end of the applied pulse. This defines an initial demagnetization region, which can be followed by a slight "remagnetization" (i.e., an increase in the z-magnetization), before entering another regime on longer time scales that, in this case, continue to demagnetize Ni up to 5 ps, as illustrated in Fig. 2b. On these longer time scales, one can also identify mild oscillations in the magnetization while it continues decreasing until it reaches about 25% of the ground state moment at 5 ps.

To characterize the effects of the laser field within the different regimes, we start by applying 50 fs pulses with different intensities. The results are shown in Fig. 2c exhibit a very rich scenario as a function of the reference laser electric field intensity $E^* = 9.7 \times 10^8$ V m^{-1}. During the initial demagnetization regime, increasing the laser intensity leads to a stronger reduction of the spin moment, while an oscillatory behavior emerges for larger times after a clear threshold around $E_0 = 6.5E^* - 6.8E^*$. These oscillations decrease in amplitude when the intensity is further increased, and the largest responses are then limited to a relatively small range of E_0 values. By increasing the laser width to 100 fs, as shown in Fig. 2d, the laser pulse switches the sign of the z-component of the magnetization. We also see that increasing the magnitude of the laser electric field leads to a stronger initial demagnetization regime and also stronger oscillation amplitudes with longer periods, the latter two becoming smaller again for $E_0 = 11E^*$. For smaller laser field intensities, the associated

switching point ($M_z = 0$) remarkably moves to earlier times. For both 50 and 100 fs widths, the dynamical dependence on the laser intensity and width is nontrivial. Certain combinations of intensities and widths keep the z-magnetization negative for a relatively long time after reversal. Moreover, the magnetization behavior strongly depends on the nature of the polarization and helicity of the laser pulse (see examples in Supplementary Fig. 1). However, the oscillatory behavior and magnetization reversal identified in panels c and d of Fig. 2 were only found for simulations where the laser electric field is circularly polarized and rotates in a plane that contains the initial orientation of the magnetic moment. Therefore, unless explicitly mentioned, in the following discussions we focus on the results obtained with pulses polarized in the yz-plane.

By extending the parameter space with systematic simulations of various pulses, we map all the switching and no-switching cases into the phase diagram shown in Fig. 1b, where the horizontal and vertical axes represent the pulse width and the absorbed laser fluence, respectively. The shaded green region illustrates the switching region, where the probability of spin reversal is high. We note that the magnetization in some cases can switch back after a few ps and then experience an oscillatory behavior. This is the time scale where the dissipation mechanisms, not included in our simulations, kick in, which we believe will help stabilize the magnetization switching. One can see from the diagram that there exists a critical minimum width for switching, which for fcc bulk Ni is about 60 fs. Once the pulse width is larger than that value, we find that there is a laser fluence window for the switching to occur where the lower bound slightly decreases and the upper-bound increases as the pulse gets wider. The requirement of a minimum intensity threshold for switching is a reasonable and expected condition since weak laser fields would not excite enough electrons to trigger strong enough dynamics to induce the switching; however, critical pulse energy to induce magnetization reversal is surprising taking into consideration the demagnetization and precession induced by the laser (and illustrated in Fig. 2c, d). In this sense, one would naively expect that higher energies would further excite the system leading to more spin moment loss and larger precession amplitude. A narrow window in the same laser parameter space was experimentally identified for Co/Pt[19]. An interesting feature in the obtained demagnetization curves is that the switching may occur while the pulse is still effective (see Supplementary Fig. 2), when the system is pumped with more energetic pulses of widths larger than 100 fs.

Laser-induced torque. The dynamics of the magnetization in each scenario are actually more complicated than its z-component in Fig. 2 can display—the transverse components also change dramatically depending on the laser characteristics. In Fig. 3, we show the 3-dimensional (3D) magnetization response to a 100 fs laser pulse with two different intensities. The lower intensity case in Fig. 3a illustrates the magnetization quickly reducing in amplitude and early on rotating in the yz-plane (as seen also from the transverse cut shown in Fig. 3b)—interestingly, the plane containing the initial state and the polarization of the laser pulse. After the fast initial demagnetization region in the yz-plane, the magnetization acquires also an x-component and rotates away from the initial plane. When increasing the laser intensity, Fig. 3c and d, the magnetization can even switch back towards the initial direction of the moment after some time.

The identified magnetization precession results from a torque induced by the laser. As we consider a bulk material and no applied magnetic field, the only torque acting on the spin magnetization $\mathbf{M} = -\gamma \langle \mathbf{S} \rangle$ is the spin–orbit torque $\mathbf{T}_{SOC} = -\gamma\lambda \langle \mathbf{L} \times \mathbf{S} \rangle$. Here γ

is the gyromagnetic ratio, λ is the spin–orbit interaction strength and $\mathbf{S}$ and $\mathbf{L}$ are the quantum-mechanical spin and orbital angular momentum operators, respectively. The expectation value is computed with the time-dependent electronic wave functions. The magnetization dynamics due to the combination of precession and demagnetization can then be written as

$$\frac{d\mathbf{M}}{dt} = \mathbf{T}_{SOC} = -\gamma\mathbf{M} \times \left(\mathbf{B}_{IFE} + \mathbf{B}_{MAE}\right) - \chi_L\mathbf{M} . \quad (1)$$

The effective field that generates the torque has two distinct contributions: $\mathbf{B}_{IFE}$ is due to an inverse Faraday-like effect (IFE) and acts only during the laser pulse, while $\mathbf{B}_{MAE}$ is due to the time-dependent magnetic anisotropy of the non-equilibrium electronic system and so also acts after the laser pulse is over. The last term is a longitudinal contribution that represents the demagnetization driven by the laser with rate χ_L and is also contained in $\mathbf{T}_{SOC}$.

We now consider a 300 fs laser pulse, in order to enhance the torque contribution which is driven directly by the laser. $\mathbf{B}_{IFE}$ is expected to point perpendicular to the polarization plane of the circular laser pulse, i.e. along the x-direction, given that the electric field rotates in the yz-plane as shown in Fig. 4a. The resulting torque points along y and enforces the observed rotation within the yz-plane. Inverting the polarization of the laser pulse changes the direction of the torque and so also the sense of rotation of the magnetization. This can be identified in Fig. 4c, d, where the total torque is plotted as a function of time. At early times, one notices that the three components of the torques are finite. The y-component of the torque acts earlier and is larger than the x-component, in line with our interpretation based on the IFE. Both components change signs by switching the polarization of the pulse. If the polarization plane is perpendicular to the ground state magnetization, as illustrated in Fig. 4b, the corresponding transverse torque cancels out (see Fig. 4e), and no rotation of the magnetization is expected as verified in our simulations. Therefore, a laser-driven torque leading to magnetization reversal is most efficient if the initial magnetization direction is contained in the plane of the circular polarization. After the laser pulse is over, the second torque shown in Eq. (1) kicks in and rotates the moment out of the yz-plane (sketched in Fig. 4f) at a time scale of the order of picoseconds, settled by the non-equilibrium magnetic anisotropy energy. We do not have a precise definition for this quantity, but as the occupations of the different electronic orbitals are strongly modified by the laser we speculate that this leads to a large modification of the effective MAE acting on the magnetic moment. The magnetization dynamics on this longer time scale are shown in Fig. 4g, where we can also identify oscillations in the magnitude of the magnetization. These hint at internal dynamics that we now discuss.

Orbital-dependent magnetization dynamics. Our method enables us to study not only the time-dependent amplitude of the total magnetization but also the internal dynamic contributions from different electronic states, as we now discuss for the same circular right-handed pulse of 300 fs width polarized in the yz plane. We compute the magnetization vectors $\mathbf{M}_{sp}$ and $\mathbf{M}_d$ carried by the sp and d orbitals, respectively, with their magnitudes and the angle between them shown in Fig. 5a. The dynamics of the z component of the magnetization contributed by each individual orbital is given in Fig. 5b and their occupations in Fig. 5c, showing the complex and rich behavior originating from each s, p and d orbital to the dynamics up to 0.4 ps. We clearly observe that the sp orbitals contribute to the magnetization dynamics on an equal footing and undergo switching similarly to the d orbitals. The most striking finding is of a transient intra-atomic non-collinear state of the sp and d magnetizations, with an effective

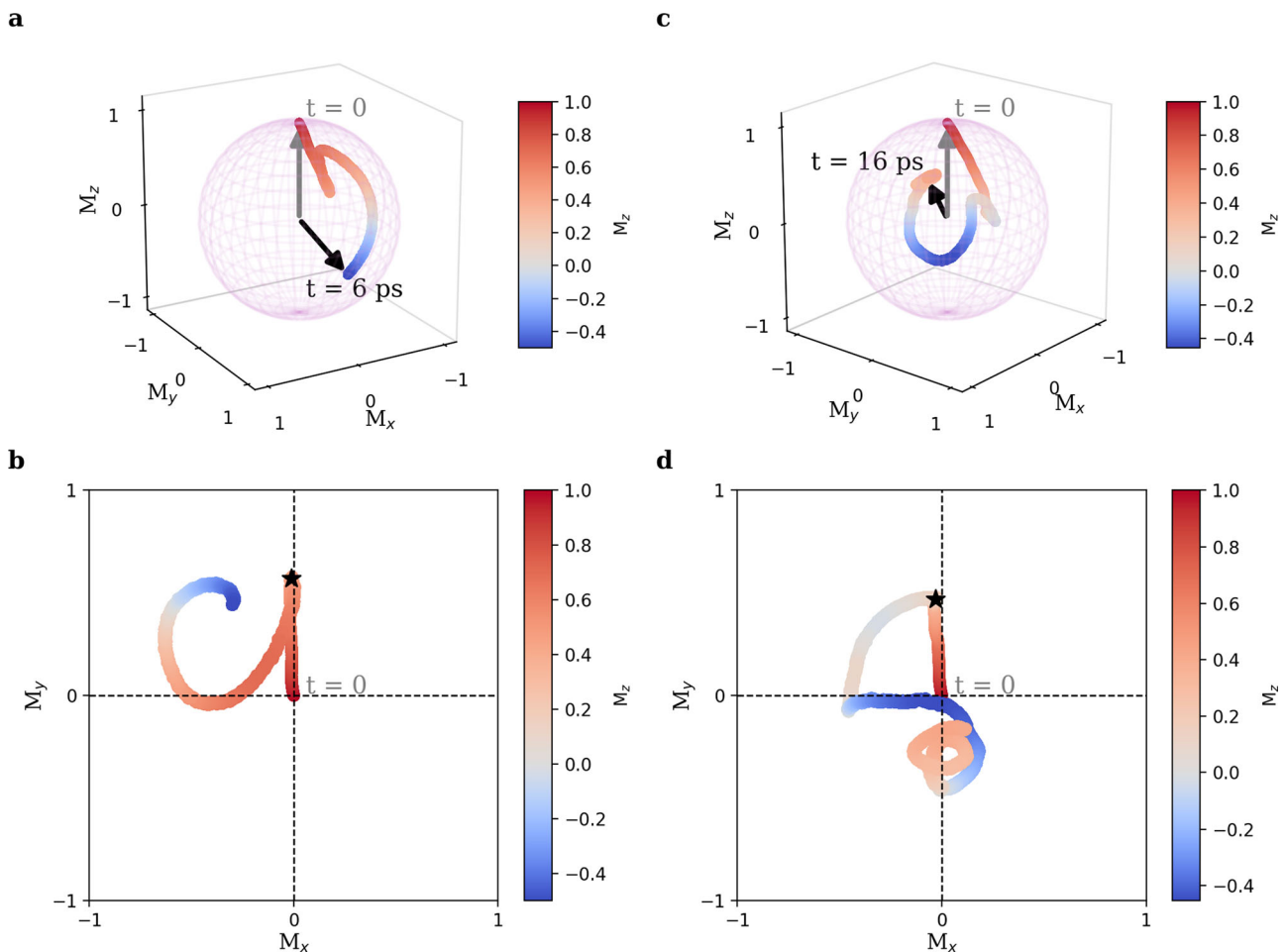**Fig. 3 Three-dimensional ultrafast magnetization dynamics of bulk Ni. a** Trajectory of the magnetization vector excited by a 100 fs pulse with the intensity of $E_0 = 6.79 \times 10^9$ V m^{-1} ($7E^*$ in Fig. 2d), with the respective associated projection on the xy-plane in (**b**). **c** Trajectory of the magnetization vector excited by a 100 fs pulse with the intensity of $E_0 = 9.7 \times 10^9$ V m^{-1} ($10E^*$ in Fig. 2d), with the respective associated projection on the xy-plane in (**d**). The color maps illustrate the z-component of the magnetization and the star indicates the end of the pulse.

ferromagnetic coupling lasting from about 60 to 165 fs, which is reminiscent of the transient ferromagnetic state of the two sub-lattices in ferrimagnetic alloys undergoing ultrafast magnetization switching[6]. After 165 fs, the coupling in the transient non-collinear state switches to antiferromagnetic, which settles in an antiferromagnetic state with weak intra-atomic non-collinearity once the laser weakens and after it ends.

We can identify three main regions with distinct dynamical behavior while the laser is acting on the material. In the first region R1, up to about 60 fs, there is a small reduction of the magnetization of the d states, while the one contributed by the sp states falls to zero at the end of this region. The dynamics of all the orbitals belonging to the respective s, p, and d groups closely follow each other, with the d_{yz} orbital starting to split from the other d orbitals (Fig. 5b), while their occupations change little (Fig. 5c). As is well known, the sp and d orbitals are antiferromagnetically coupled to each other in the ground state[52], but surprisingly the transition to the next dynamical region is accompanied by a strong noncollinearity of $\mathbf{M}_{sp}$ and $\mathbf{M}_d$ (Fig. 5a). In the second dynamical region R2, from about 60–165 fs, there is a strong collapse of the magnetization of the d states accompanied by a strong increase of the magnetization of the sp states (Fig. 5a). The angle between the two magnetization vectors varies in a complex way and their coupling becomes ferromagnetic-like, with an accompanying rotational motion of the total magnetization vector in the yz-plane. The switching of the z component of the

magnetization occurs due to the large transfer of spin angular momentum from the d to the sp states (Fig. 5a), which is now also accompanied by a large transfer of orbital population (Fig. 5c). At the end of this region, the d magnetization is minimal and is in the process of rotating from being parallel to being antiparallel to the larger magnetization now displayed by the sp states. In the third dynamical region R3, from about 165 fs to essentially the end of the laser pulse, the d magnetization partly recovers and assumes an almost antiparallel alignment to the sp one (Fig. 5a). The orbital occupations stabilize (Fig. 5c), but the d orbitals develop internal oscillations with a short period of tens of femtoseconds, which continue after the laser is over (Fig. 5b).

The previous observations lead us to propose the following physical picture for the different dynamical processes actively driven by the laser pulse, as illustrated in Fig. 5d–f. In the first demagnetization region R1 up to 60 fs, intra-orbital spin–flip processes, i.e. within each orbital channel (d–d), (sp–sp) are responsible for the initial reduction of the magnetization until the spin moment of the sp-electrons is fully quenched (Fig. 5d). Both the mechanism and the time scale are explained by SOC. In the second region R2 starting after 60 fs, inter-orbital optical transitions become important while maintaining strong intra-atomic noncollinearity with the sp and d moments entering a transient ferromagnetic coupling and reaching similar magnitudes (Fig. 5e). Here the time scale is set by effective inter-orbital
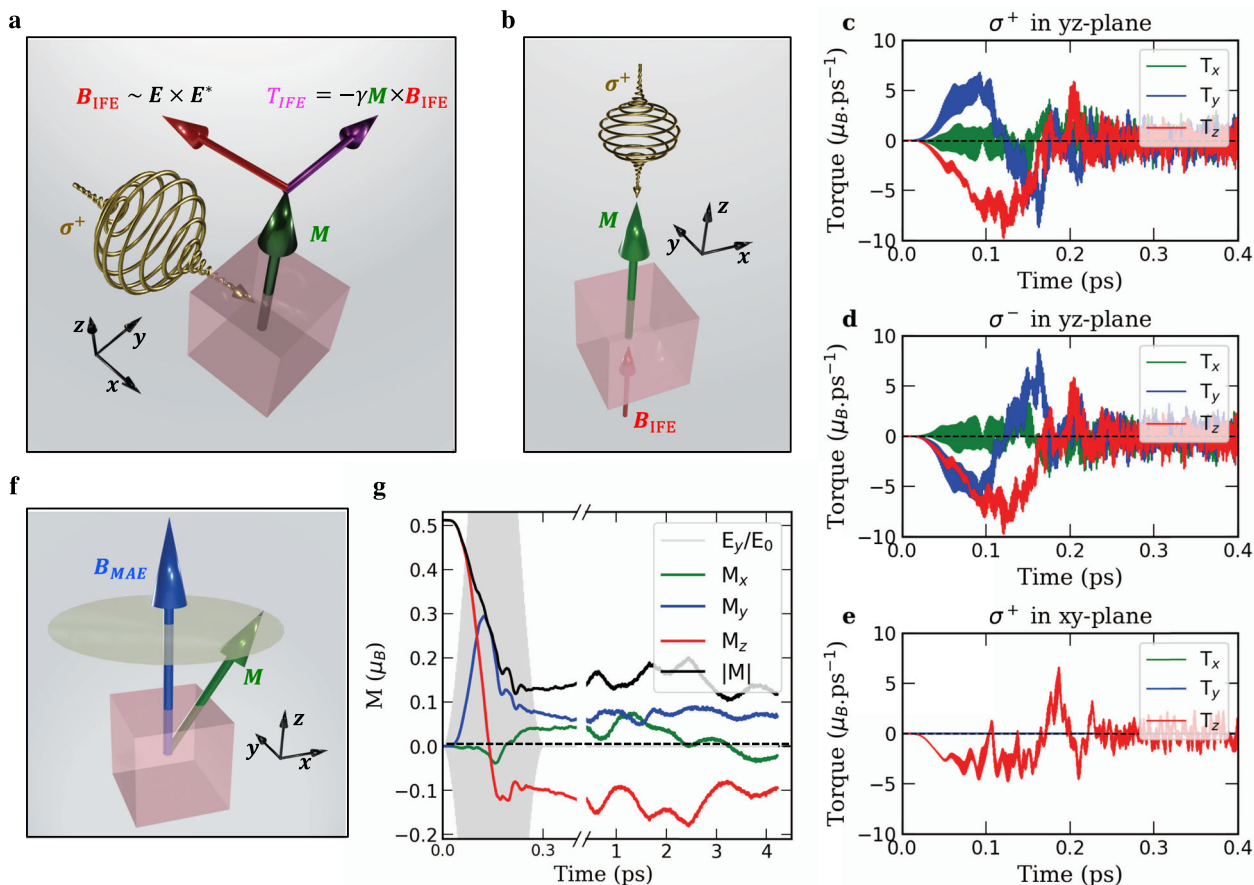
Fig. 4 Laser-induced ultrafast magnetic torques on bulk Ni. a, **b** Schematic illustrations representing a laser acting on an initial magnetization along the z-axis: (**a**) a right-circularly polarized pulse (σ^+) in the yz-plane induces an inverse Faraday-like magnetic field ($\mathbf{B}_{IFE}$) opposite to the polarisation direction ($-x$), which at $t = 0$ exerts a torque ($\mathbf{T}_{IFE}$) on the magnetization ($\mathbf{M}$) along the $+y$ direction; (**b**) a right-circularly polarized pulse in the xy-plane would generate an inverse Faraday-like magnetic field parallel to the magnetization ($+z$) and so at $t = 0$ it exerts no torque. **c–e** The components of the torques induced by a 300 fs wide pulse with the intensity of $E_0 = 9.7 \times 10^9$ V m^{-1} that is **c** right-circularly polarized in the yz-plane, **d** left-circularly polarized (σ^-) in the yz-plane, and **e** right-circularly polarized in the xy-plane, respectively, computed according to Eq. (1). **f** The magnetization dynamics also have a contribution from the internal field due to the magnetic anisotropy (MAE) which induces precession. **g** The three components of magnetization ($\mathbf{M}$) along with the total length correspond to the case shown in (**c**).

exchange interactions. The nature of the effective inter-orbital exchange coupling changes due to the orbital repopulation. After 165 fs (R3), a new equilibrium between the occupations of the orbitals is reached, which recovers the initial inter-orbital antiferromagnetic coupling, enforcing the weaker moment (which is now the d-magnetization) to point in the opposite direction to the stronger one originating from the sp states (Fig. 5g). There is also a significant remagnetisation of the d orbitals which could be driven by the coupling to the larger magnetization of the sp orbitals and is assisted by the laser (Fig. 5a). To summarize, the demagnetization rate of both types of electrons is not the same since the strength of the matrix elements responsible for the spin–orbit-driven spin–flip processes is orbital dependent. When both families of orbitals are demagnetized, the strong population switching of the electronic states in favor of the sp-type forces the d-electrons to have their moments growing in the direction opposite than that of the sp-electrons when their natural inter-orbital antiferromagnetic coupling is restored.

Conclusion

In conclusion, we predict via time-dependent electronic structure simulations that the so-far elusive magnetization switching in an elementary ferromagnet such as bulk fcc Ni is possible with a single

laser pulse. We mapped the laser-pulse parameter regime enabling the reversal of the magnetization and found that a minimum pulse width of 60 fs is required while increasing the pulse width widens the laser fluence range allowing all-optical manipulation of the direction of the magnetization. The magnetization reversal is enabled by laser-driven torques that rotate their orientation together with the usual demagnetization process and require the proper selection of a laser pulse that is circularly polarized in a plane containing the ground-state magnetization. Our simulations unveiled complex and rich orbital magnetization dynamics with transient intra-atomic non-collinear states and unexpectedly fast precessional dynamics which we attribute to the nonequilibrium magnetic anisotropy created by the laser-induced electronic repopulation. Even though relaxation mechanisms were not incorporated in our simulations, we conjecture that adding a dissipation channel (for instance due to electron–phonon coupling) would both enhance the computed demagnetization and dampen the laser-driven precession without qualitatively affecting our main findings[43–45], i.e. the presence of complex intra-atomic spin dynamics together with the light-induced torque, which if correctly positioned can efficiently switch the magnetization of an elementary ferromagnet. We envision that our results will promote further studies focusing on the polarisation-dependent all-optical magnetization reversal and even in characterizing intriguing inter-orbital
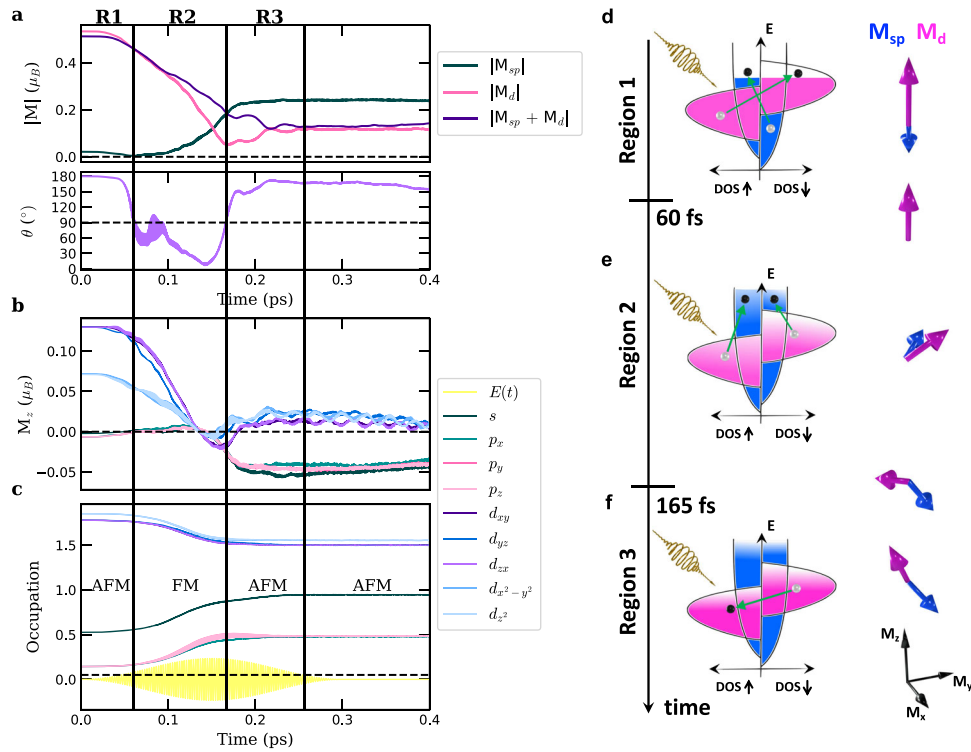
Fig. 5 Orbital dependence of the ultrafast magnetization dynamics of bulk Ni. a The length of the magnetization vectors for the *sp* and d orbitals along with their vector sum and the angle θ between the magnetization vectors of the *sp* and d orbitals. **b** The orbital contributions to the *z* component of the magnetization. **c** The occupation of the *sp* and d orbitals. The vertical lines indicate the identified three regimes of demagnetization. **d–f** Schematics of the magnetization dynamics for the different regimes. The diagrams on the left column indicate the main electronic processes while those on the right illustrate the evolution of the noncollinear intra-atomic magnetic moments. In this simulation, the width of the laser pulse was 300 fs and its intensity $E_0 = 9.7 \times 10^9 \, \text{V m}^{-1}$.

intra-atomic transient complex magnetic states. Such findings open further perspectives in the implementation of all-optical addressed spintronic storage and memory devices.

Methods

Theory. We utilize a multi-orbital tight-binding Hamiltonian that takes into account the electron–electron interaction through a Hubbard-like term and the spin–orbit interaction, as implemented on the TITAN code to investigate dynamics of transport and angular momentum properties in nanostructures[53–56]. To describe the interaction of a laser pulse with the system, we include a time-dependent electric field described by a vector potential $\mathbf{A}(t) = -\int \mathbf{E}(t)\mathrm{d}t$. The full Hamiltonian is given by

$$\mathcal{H}(t) = \mathcal{H}_{\text{kin}} + \mathcal{H}_{\text{xc}} + \mathcal{H}_{\text{soc}} - \int d\mathbf{r} \, \hat{\mathbf{J}}^{\text{C}}(\mathbf{r}, t) \cdot \mathbf{A}(\mathbf{r}, t) \, . \quad (2)$$

More details on each term can be found in Supplementary Note 1. The dipole approximation was used in the implementation of the vector potential, meaning that the spatial dependency is not included since the wavelength of the used light ($\hbar\omega = 1.55 \, \text{eV} \rightarrow \lambda = 800 \, \text{nm}$) is much larger than the lattice constant and that the quadratic term as well as the other higher terms are zero[57]. We approximate the absorbed laser fluence by the change in the energy of the system divided by its cross-section

$$\text{absorbed laser fluence} = \frac{\langle\mathcal{H}\rangle(t) - \langle\mathcal{H}\rangle(0)}{a^2} \, , \quad (3)$$

where *a* is the lattice constant. This approaches a stable value after the end of the laser pulse.

Pulse shape. For the right-handed circular pulse (σ^+) polarized in the *yz*-plane, for example, the pulse shape is described using a vector potential of the following form[58]:

$$\mathbf{A}(t) = -\frac{E_0}{\omega} \cos^2(\pi t/\tau)[\sin(\omega t)\hat{\mathbf{y}} - \cos(\omega t)\hat{\mathbf{z}}], \quad (4)$$

where E_0 is the electric field intensity, τ is the pulse width, ω is the laser central frequency which is set to 1.55 eV $\hbar^{-1}$. The magnetic field of the laser is neglected since it is much smaller than the electric field.

For the linear pulse (π) of a propagation direction along the diretion $\hat{\mathbf{u}}$, using the same central frequency, the vector potential is described as

$$\mathbf{A}(t) = -\frac{E_0}{\omega} \cos^2(\pi t/\tau) \sin(\omega t)\hat{\mathbf{u}} \, . \quad (5)$$

Computational details. Calculations were performed on bulk face-centered cubic Nickel using the theoretical lattice constant of 3.46 Å given in ref. [59], one atom in the unit cell for all calculations, a uniform *k*-point grid of (22 × 22 × 22) and a temperature of 496 K in the Fermi–Dirac distribution. The initial step size for the time propagation is $\Delta t = 1$ a.u. which changes in the subsequent steps to a new predicted value such that a relative and an absolute error in the calculated wave functions stay smaller than 10^{-3} [60].

We tested the results for accuracy by increasing the number of *k*-points and decreasing the tolerance for the relative and absolute errors. The method was also tested for stability by changing one of the laser parameters by a very small number while keeping the other parameters fixed, for one case that we already have results for. The results then were not very different[61].

Data availability
The data that support the findings of this study are available from the corresponding authors on request.

Code availability
The tight-binding code that supports the findings of this study, TITAN, is available from the corresponding author on request.

References
1. Beaurepaire, E., Merle, J. -C., Daunois, A. & Bigot, J. -Y. Ultrafast spin dynamics in ferromagnetic nickel. *Phys. Rev. Lett.* **76**, 4250 (1996).

2. Stanciu, C. et al. All-optical magnetic recording with circularly polarized light. *Phys. Rev. Lett.* **99**, 047601 (2007).
3. Lambert, C.-H. et al. All-optical control of ferromagnetic thin films and nanostructures. *Science* **345**, 1337–1340 (2014).
4. John, R. et al. Magnetisation switching of FePt nanoparticle recording medium by femtosecond laser pulses. *Sci. Rep.* **7**, 4114 (2017).
5. Wietstruk, M. et al. Hot-electron-driven enhancement of spin-lattice coupling in Gd and Yb 4f ferromagnets observed by femtosecond x-ray magnetic circular dichroism. *Phys. Rev. Lett.* **106**, 127401 (2011).
6. Radu, I. et al. Transient ferromagnetic-like state mediating ultrafast reversal of antiferromagnetically coupled spins. *Nature* **472**, 205–208 (2011).
7. Alebrand, S., Hassdenteufel, A., Steil, D., Cinchetti, M. & Aeschlimann, M. Interplay of heating and helicity in all-optical magnetization switching. *Phys. Rev. B* **85**, 092401 (2012).
8. Khorsand, A. R. et al. Role of magnetic circular dichroism in all-optical magnetic recording. *Phys. Rev. Lett.* **108**, 127205 (2012).
9. Ostler, T. A. et al. Ultrafast heating as a sufficient stimulus for magnetization reversal in a ferrimagnet. *Nat. Commun.* **3**, 666 (2012).
10. Graves, C. et al. Nanoscale spin reversal by non-local angular momentum transfer following ultrafast laser excitation in ferrimagnetic GdFeCo. *Nat. Mater.* **12**, 293–298 (2013).
11. Hassdenteufel, A. et al. Thermally assisted all-optical helicity dependent magnetic switching in amorphous $Fe_{100-x}Tb_x$ alloy films. *Adv. Mater.* **25**, 3122–3128 (2013).
12. Davies, C. S. et al. Exchange-driven all-optical magnetic switching in compensated 3d ferrimagnets. *Phys. Rev. Res.* **2**, 032044 (2020).
13. van Hees, Y. L., van de Meugheuvel, P., Koopmans, B. & Lavrijsen, R. Deterministic all-optical magnetization writing facilitated by non-local transfer of spin angular momentum. *Nat. Commun.* **11**, 1–7 (2020).
14. Boeglin, C. et al. Distinguishing the ultrafast dynamics of spin and orbital moments in solids. *Nature* **465**, 458–461 (2010).
15. Vodungbo, B. et al. Indirect excitation of ultrafast demagnetization. *Sci. Rep.* **6**, 1–9 (2016).
16. Vomir, M., Albrecht, M. & Bigot, J.-Y. Single shot all optical switching of intrinsic micron size magnetic domains of a Pt/Co/Pt ferromagnetic stack. *Appl. Phys. Lett.* **111**, 242404 (2017).
17. Shokeen, V. et al. Spin flips versus spin transport in nonthermal electrons excited by ultrashort optical pulses in transition metals. *Phys. Rev. Lett.* **119**, 107203 (2017).
18. Siegrist, F. et al. Light-wave dynamic control of magnetism. *Nature* **571**, 240–244 (2019).
19. Kichin, G. et al. From multiple-to single-pulse all-optical helicity-dependent switching in ferromagnetic co/pt multilayers. *Phys. Rev. Appl.* **12**, 024019 (2019).
20. Yamada, K. T. et al. Efficient all-optical helicity-dependent switching in pt/co/pt with dual laser pulses. Preprint at bioRxiv https://arxiv.org/abs/1903.01941 (2019).
21. Cheng, F. et al. All-optical manipulation of magnetization in ferromagnetic thin films enhanced by plasmonic resonances. *Nano Lett.* **20**, 6437–6443 (2020).
22. Cheng, F. et al. All-optical helicity-dependent switching in hybrid metal–ferromagnet thin films. *Adv. Opt. Mater.* **8**, 2000379 (2020).
23. Abendroth, J. M. et al. Helicity-preserving metasurfaces for magneto-optical enhancement in ferromagnetic [Pt/Co]n films. *Adv. Opt. Mater.* **8**, 2001420 (2020).
24. Kirilyuk, A., Kimel, A. V. & Rasing, T. Ultrafast optical manipulation of magnetic order. *Rev. Mod. Phys.* **82**, 2731 (2010).
25. Koopmans, B. et al. Explaining the paradoxical diversity of ultrafast laser-induced demagnetization. *Nat. Mater.* **9**, 259–265 (2010).
26. Walowski, J. & Münzenberg, M. Perspective: ultrafast magnetism and thz spintronics. *J. Appl. Phys.* **120**, 140901 (2016).
27. Wang, C. & Liu, Y. Ultrafast optical manipulation of magnetic order in ferromagnetic materials. *Nano Convergence* **7**, 1–16 (2020).
28. El Hadri, M. S. et al. Two types of all-optical magnetization switching mechanisms using femtosecond laser pulses. *Phys. Rev. B* **94**, 064412 (2016).
29. Koopmans, B., Van Kampen, M., Kohlhepp, J. & De Jonge, W. Ultrafast magneto-optics in nickel: Magnetism or optics? *Phys. Rev. Lett.* **85**, 844 (2000).
30. Koopmans, B., Ruigrok, J., Dalla Longa, F. & De Jonge, W. Unifying ultrafast magnetization dynamics. *Phys. Rev. Lett.* **95**, 267207 (2005).
31. Mekonnen, A. et al. Role of the inter-sublattice exchange coupling in short-laser-pulse-induced demagnetization dynamics of GdCo and GdCoFe alloys. *Phys. Rev. B* **87**, 180406 (2013).
32. Atxitia, U. & Chubykalo-Fesenko, O. Ultrafast magnetization dynamics rates within the Landau–Lifshitz–Bloch model. *Phys. Rev. B* **84**, 144414 (2011).
33. Mentink, J. H. et al. Ultrafast spin dynamics in multisublattice magnets. *Phys. Rev. Lett.* **108**, 057202 (2012).
34. Kimel, A. et al. Ultrafast non-thermal control of magnetization by instantaneous photomagnetic pulses. *Nature* **435**, 655–657 (2005).
35. Tesařová, N. et al. Experimental observation of the optical spin–orbit torque. *Nat. Photonics* **7**, 492–498 (2013).
36. Berritta, M., Mondal, R., Carva, K. & Oppeneer, P. M. Ab initio theory of coherent laser-induced magnetization in metals. *Phys. Rev. Lett.* **117**, 137203 (2016).
37. Zhang, G., Bai, Y. & George, T. F. Switching ferromagnetic spins by an ultrafast laser pulse: emergence of giant optical spin–orbit torque. *Europhys. Lett.* **115**, 57003 (2016).
38. Huisman, T. et al. Femtosecond control of electric currents in metallic ferromagnetic heterostructures. *Nat. Nanotechnol.* **11**, 455–458 (2016).
39. Freimuth, F., Blügel, S. & Mokrousov, Y. Laser-induced torques in metallic ferromagnets. *Phys. Rev. B* **94**, 144432 (2016).
40. Choi, G.-M., Schleife, A. & Cahill, D. G. Optical-helicity-driven magnetization dynamics in metallic ferromagnets. *Nat. Commun.* **8**, 15085 (2017).
41. Battiato, M., Carva, K. & Oppeneer, P. M. Superdiffusive spin transport as a mechanism of ultrafast demagnetization. *Phys. Rev. Lett.* **105**, 027203 (2010).
42. Stamm, C. et al. Femtosecond modification of electron localization and transfer of angular momentum in nickel. *Nat. Mater.* **6**, 740–743 (2007).
43. Carva, K., Battiato, M. & Oppeneer, P. M. Ab initio investigation of the Elliott–Yafet electron–phonon mechanism in laser-induced ultrafast demagnetization. *Phys. Rev. Lett.* **107**, 207201 (2011).
44. Chen, Z. & Wang, L.-W. Role of initial magnetic disorder: a time-dependent ab initio study of ultrafast demagnetization mechanisms. *Sci. Adv.* **5**, eaau8000 (2019).
45. Maldonado, P. et al. Tracking the ultrafast nonequilibrium energy flow between electronic and lattice degrees of freedom in crystalline nickel. *Phys. Rev. B* **101**, 100302 (2020).
46. Töws, W. & Pastor, G. Many-body theory of ultrafast demagnetization and angular momentum transfer in ferromagnetic transition metals. *Phys. Rev. Lett.* **115**, 217204 (2015).
47. Krieger, K., Dewhurst, J., Elliott, P., Sharma, S. & Gross, E. Laser-induced demagnetization at ultrashort time scales: predictions of Tddft. *J. Chem. Theory Comput.* **11**, 4870–4874 (2015).
48. Krieger, K. et al. Ultrafast demagnetization in bulk versus thin films: an ab initio study. *J. Phys.: Condens. Matter* **29**, 224001 (2017).
49. Simoni, J., Stamenova, M. & Sanvito, S. Ultrafast demagnetizing fields from first principles. *Phys. Rev. B* **95**, 024412 (2017).
50. Elliott, P. et al. The microscopic origin of spin–orbit mediated spin-flips. *J. Magn. Magn. Mater.* **502**, 166473 (2020).
51. Scheid, P., Sharma, S., Malinowski, G., Mangin, S. & Lebègue, S. Ab initio study of helicity-dependent light-induced demagnetization: from the optical regime to the extreme ultraviolet regime. *Nano Lett.* **21**, 1943–1947 (2021).
52. Akai, H. et al. Theory of hyperfine interactions in metals. *Prog. Theor. Phys. Suppl.* **101**, 11–77 (1990).
53. Guimarães, F. S. M., Lounis, S., Costa, A. T. & Muniz, R. B. Dynamical current-induced ferromagnetic and antiferromagnetic resonances. *Phys. Rev. B* **92**, 220410 (2015).
54. Guimarães, F. S. et al. Dynamical amplification of magnetoresistances and hall currents up to the THz regime. *Sci. Rep.* **7**, 1–9 (2017).
55. Guimarães, F. S. et al. Comparative study of methodologies to compute the intrinsic gilbert damping: interrelations, validity and physical consequences. *J. Phys.: Condens. Matter* **31**, 255802 (2019).
56. Guimarães, F. S., Bouaziz, J., dos Santos Dias, M. & Lounis, S. Spin–orbit torques and their associated effective fields from gigahertz to terahertz. *Commun. Phys.* **3**, 1–7 (2020).
57. Chen, Z., Luo, J.-W. & Wang, L.-W. Revealing angular momentum transfer channels and timescales in the ultrafast demagnetization process of ferromagnetic semiconductors. *Proc. Natl Acad. Sci. USA* **116**, 19258–19263 (2019).
58. Volkov, M. et al. Attosecond screening dynamics mediated by electron localization in transition metals. *Nat. Phys.* **15**, 1145–1149 (2019).
59. Papaconstantopoulos, D. A. *Handbook of the Band Structure of Elemental Solids* (Springer US, 2015).
60. Hairer, E. & Wanner, G. *Solving Ordinary Differential Equations II: Stiff and Differential-Algebraic Problems. Springer Series in Computational Mathematics* (Springer-Verlag, 2010).
61. Higham, N. J. *Accuracy and Stability of Numerical Algorithms* (SIAM, 2002).
62. Jülich Supercomputing Centre. JURECA: modular supercomputer at Jülich Supercomputing Centre. *J. Large-scale Res. Facil.* **4** https://doi.org/10.17815/jlsrf-4-121-1 (2018).

Acknowledgements

Author contributions

H.H. performed the calculations and implemented the time evolution method under the supervision of F.S.M.G. and M.d.S.D. S.L. initiated, designed, and supervised the project. All the authors discussed the obtained results and contributed to writing and revising the manuscript.

Competing interests

The authors declare no competing interests.

Additional information

Supplementary information The online version contains supplementary material available at https://doi.org/10.1038/s42005-021-00798-8.

Correspondence and requests for materials should be addressed to Hanan Hamamera or Samir Lounis.

Peer review information *Communications Physics* thanks the anonymous reviewers for their contribution to the peer review of this work. Peer reviewer reports are available.

Reprints and permission information is available at http://www.nature.com/reprints

Publisher's note Springer Nature remains neutral with regard to jurisdictional claims in published maps and institutional affiliations.